Technical Material

Nuclear data-induced uncertainty quantification of prompt neutron decay constant based on perturbation theory for ADS experiments at KUCA

Tomohiro Endo[a*], Kenichi Watanabe[a], Go Chiba[b] Masao Yamanaka[c],

Willem Frederik Geert van Rooijen[d], Cheol Ho Pyeon[c]

[a] *Department of Applied Energy, Graduate School of Engineering, Nagoya University, Furo-cho, Chikusa-ku, Nagoya, Aichi, 464-8603, Japan;*

[b] *Division of Energy and Environmental Systems, Graduate School of Engineering, Hokkaido University, Kita 13, Nishi 8, Kita-ku, Sapporo, Hokkaido, 060-8628, Japan;*

[c] *Research Center for Safe Nuclear System, Institute for Integrated Radiation and Nuclear Science, Kyoto University, Asashiro-nishi, Kumatori-cho, Sennan-gun, Osaka, 590-0494, Japan;*

[d] *Department of Nuclear Reactor Physics, Research Institute of Nuclear Engineering, University of Fukui, 1-3-33 Kanawa-cho, Tsuruga-shi, Fukui, 914-0055, Japan*

Abstract

In experimental benchmarks of the accelerator-driven system (ADS) conducted at the Kyoto University Critical Assembly (KUCA), the prompt neutron decay constant α was measured using two types of pulsed neutron sources, i.e. a D-T neutron source and a spallation neutron source driven by a 100-MeV proton beam. The measurement results of α are useful information to validate the numerical results predicted by the prompt ω-eigenvalue calculation. In this study, the numerical analysis of α using a multi-energy group S_N neutron transport code was carried out for the uranium-lead zoned experimental cores. To reduce the discretization error owing to the deterministic code, the KUCA geometry was modelled in detail as a three-

*Corresponding author. Email: t-endo@energy.nagoya-u.ac.jp

dimensional heterogeneous plate-by-plate geometry, and an improved variant of EO_N quadrature was utilized. In addition, the sensitivity coefficients of α with respect to nuclear data were efficiently evaluated by first-order perturbation theory, followed by nuclear data-induced uncertainty quantification based on the 56 neutron-energy group SCALE covariance library. Consequently, the numerical results of α were validated successfully by the experimental results of the pulsed neutron source method, compared with the range of the nuclear data-induced uncertainties.

Keywords: prompt neutron decay constant; KUCA; ADS; measurement; ω-eigenvalue; sensitivity analysis; uncertainty quantification

1. Introduction

Accelerator-driven systems (ADSs) have been investigated for transmuting minor actinides and long-lived radioactive fission products. Towards the realization of ADS, research on the subcriticality measurement technique is important to confirm experimentally whether the neutron multiplication in the system has a sufficient margin to criticality. Because of the subcritical characteristic of ADS, the subcriticality $-\rho \equiv (1 - k_{\text{eff}})/k_{\text{eff}}$ cannot be directly obtained by the reactivity difference from just the critical state ($k_{\text{eff}} = 1$), where k_{eff} is the effective neutron multiplication factor. Instead, the subcriticality is indirectly measured via other measurable core characteristics parameters, e.g. the prompt neutron decay constant α.

Various ADS experiments were conducted at the Kyoto University Critical Assembly (KUCA), and the experimental benchmarks were published for the validation of a neutron transport calculation code [1,2,3,4,5,6]. For example, the prompt neutron decay constant α was measured as a kinetic parameter, using either a D-T neutron source or a spallation neutron source generated by a 100-MeV proton beam from the fixed-field alternating gradient (FFAG) accelerator [7,8] impinging on a heavy metal target, e.g. lead-bismuth (Pb-Bi). As reported in previous research [9], the experimental values of α are useful information to validate the ω-eigenvalue calculation, which gives the reciprocal of the time constant in the temporal variation of the neutron flux $\psi(t) \propto \exp(\omega t)$. The numerically predicted values have uncertainties due to the analytical modelling error (e.g. discretization error owing to a deterministic code) and the uncertainty of input parameters (e.g. covariance data of nuclear data). Thus, the sensitivity analysis (SA) and the uncertainty quantification (UQ) for the numerical results of α are also important for the best estimate plus uncertainty.

In previous research, the uncertainty quantification of α was accomplished by the random-sampling technique [9]. Although the random-sampling technique makes it possible to carry out UQ simply for arbitrary types of target parameters, the statistical error is inevitable. For example, if the probability distribution of the target parameter follows the normal

distribution, the relative statistical error of uncertainty evaluated by the random-sampling technique can be estimated by $\sqrt{1-\frac{2}{N-1}\left(\frac{\Gamma(N/2)}{\Gamma((N-1)/2)}\right)^2} \approx 1/\sqrt{2(N-1)}$, where N is the number of samplings and $\Gamma(x)$ is the gamma function. Consequently, the longer calculation time is necessary to obtain the uncertainty with the smaller statistical error. In addition, the estimation of the fine structure of sensitivity coefficients becomes more difficult owing to the statistical error, as the number of neutron energy groups increases. Recently, an efficient numerical calculation method for SA of α was proposed based on the first-order perturbation theory (PT) [10]. In the case of PT, only two ω-eigenvalue calculations are needed, i.e. one forward calculation and one adjoint calculation, to evaluate sensitivity coefficients of α with respect to arbitrary nuclear data (e.g. microscopic cross section, prompt fission spectrum χ_{p}, number of prompt neutrons per fission ν_{p}). In Reference [10], the verification of PT-based SA was conducted for a simple spherical critical core (HEU-SOL-THERM-012 in ICSBEP [11]). Thus, further investigations are desirable for more-complicated actual experimental cores.

The KUCA ADS benchmark problems define detailed, three-dimensional, heterogeneous core geometries. In previous studies, the PT-based SA and UQ were investigated from the viewpoint of k_{eff} [2,12]. The aim of this study is to clarify the major contributions to the nuclear data-induced uncertainty of the prompt neutron decay constant α in the KUCA ADS benchmark problems. For this purpose, the efficient PT-based SA and UQ of α was applied to the KUCA ADS benchmark problems. Furthermore, by comparing the bias between numerical and experimental values of α with the nuclear data-induced uncertainty of α, this study is aimed at validating the numerical results of α.

The remainder of the work is structured as follows. In Section 2, the target of KUCA ADS benchmark problems, uranium-lead (U-Pb) cores, are briefly explained. In Section 3, the calculation conditions of deterministic neutron transport calculations using

SCALE6.2.3/CENTRM [13,14] and PARTISN [15] are presented, followed by the numerical results and discussion of Section 4. Finally, concluding remarks are presented in Section 5.

2. Experiment

2.1. Core configuration

In this study, the U-Pb zoned cores in the KUCA ADS benchmarks [6] were investigated. Because the detailed information was described in Reference [6], brief explanations are presented in this section.

Figure 1 presents the top view of the experimental cores. By substituting polyethylene reflector assemblies for fuel ones, the total number of 1/16" highly enriched uranium-aluminum alloy (HEU) plates in the subcritical core was decreased to deepen the subcriticality $-\rho$. In this study, the following six subcritical cores were numerically investigated: 4440, 4320, 4200, 4080, 3960, and 3840 HEU-plates cores. In these experiments, two types of fuel assemblies were used, i.e. a 'normal' fuel assembly, in which the fuel zone consists of 60 unit cells, each cell containing two HEU plates 1/8" thick, and one polyethylene plate 1/8" thick; the other fuel assembly consists of 40 special unit cells, each having two HEU plates 1/8" thick and one Pb plate 1/8" thick, sandwiched between 10 normal unit cells on the top and 10 normal unit cells at the bottom. Since the normal and special unit cells have the same size and number of material plates, the three-dimensional core analysis using a deterministic neutron transport calculation can be carried out by the heterogeneous 'plate-by-plate' geometrical modelling without treatment of staggered spatial meshes. In the two fuel assemblies, the 60 unit cells were axially surrounded by lower and upper polyethylene reflectors. All the six control rods were fully withdrawn in these six subcritical cores; therefore, the 1/2 core symmetry condition was reasonably applicable to the evaluation of integral experiment parameters, such as the effective neutron multiplication factor k_{eff} and α.

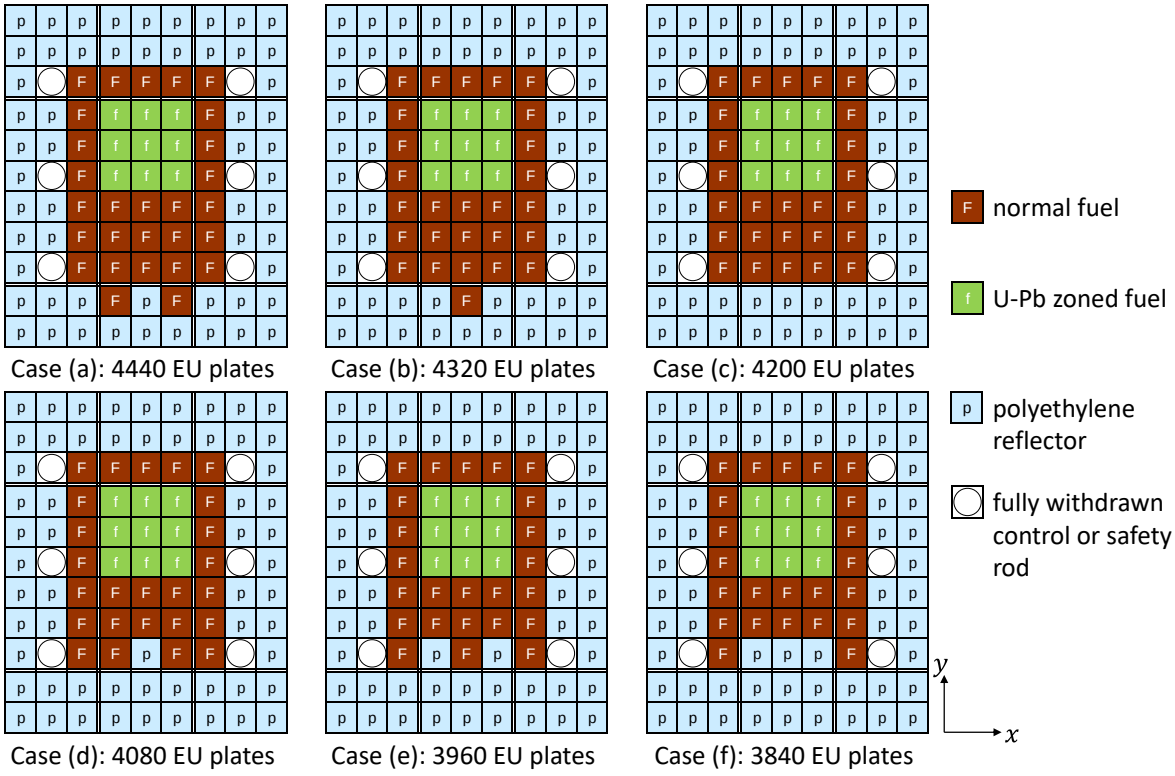

Figure 1. Top view of U-Pb zoned experimental cores.

2.2. Prompt neutron decay constant

In a series of experiments, the measurement values of the prompt neutron decay constant α were obtained using the following two types of pulsed neutron sources (PNSs): a 14-MeV neutron source generated by a D-T reaction and a spallation neutron source using 100-MeV protons with a lead-bismuth (Pb-Bi) target. In Reference [6], the two measurement values of α were available for the validation: the fitting method to the PNS histogram (or the PNS method) [16] and the Feynman-α method [17]. In this study, the measurement values using the PNS method were chosen, because the α value can be just estimated from the exponential decay of neutron count rates after the pulsed neutron injection, and the experimental errors were smaller than those of the Feynman-α method. One or more PNS experiments were conducted for each subcritical core using the D-T or spallation source. Furthermore, because there were several neutron detectors (BF_3 detectors at the axial centre positions in the polyethylene-reflector region, and optical-fibre [18] and LiCAF-fibre [19] detectors), some measurement values of α were

reported for these detectors. To evaluate a representative value of α for each subcritical core, a weighted arithmetic mean μ_α and standard deviation (square root of weighted sample variance) s_α were calculated as follows.

$$\mu_\alpha = \frac{\sum_{i=1}^{N} w_i \alpha_i}{\sum_{i=1}^{N} w_i}, \tag{1}$$

$$s_\alpha = \sqrt{\frac{\sum_{i=1}^{N} w_i (\alpha_i - \mu)^2}{\sum_{i=1}^{N} w_i - \left(\frac{\sum_{i=1}^{N} w_i^2}{\sum_{i=1}^{N} w_i}\right)}}, \tag{2}$$

$$w_i = \frac{1}{\sigma_{\alpha,i}^2}, \tag{3}$$

where α_i and $\sigma_{\alpha,i}$ are the ith measurement value of α and the fitting error, respectively; w_i is an ith weight, which is inversely proportional to $\sigma_{\alpha,i}^2$; and N is the total number of α_i values measured by different detectors over one or more times for a subcritical core. The μ_α value was expected to mitigate the spatial dependency on the fitting value of α owing to the detector position. The s_α value was used to quantify the dispersion of α_i.

3. Numerical Analysis

3.1. Theory

In general, the absolute value of the prompt neutron decay constant is much larger than the decay constant of the delayed neutron precursor, i.e. $|\alpha| \gg \max(\lambda_i)$, where λ_i is the decay constant of the ith group delayed neutron precursor. Consequently, the α value can be reasonably evaluated by the following prompt ω-eigenvalue calculation [9,10].

$$(\mathbf{F}_\mathrm{p} - \mathbf{A})\psi_{\mathrm{p},g}(\vec{r},\vec{\Omega}) = \frac{\omega_\mathrm{p}}{\mathrm{v}_g}\psi_{\mathrm{p},g}(\vec{r},\vec{\Omega}) = -\frac{\alpha}{\mathrm{v}_g}\psi_{\mathrm{p},g}(\vec{r},\vec{\Omega}), \tag{4}$$

$$\mathbf{A} \equiv \vec{\Omega}\nabla + \Sigma_{\mathrm{t},g} - \sum_{g'=1}^{NG}\sum_{l=0}^{NL}\frac{2l+1}{4\pi}\Sigma_{\mathrm{s},l,g'\to g}\sum_{m=-l}^{l} R_{l,m}(\vec{\Omega})\int_{4\pi} d\Omega' R_{l,m}(\vec{\Omega}'), \tag{5}$$

$$\mathbf{F}_{\mathrm{p}} \equiv \frac{\chi_{\mathrm{p},g}}{4\pi} \sum_{g'=1}^{NG} \nu_{\mathrm{p}} \Sigma_{\mathrm{f},g'}\,, \tag{6}$$

where $\mathbf{A}$ and $\mathbf{F}_{\mathrm{p}}$ are the net neutron loss and prompt neutron production operators, respectively; $\Sigma_{\mathrm{t},g}$, $\Sigma_{\mathrm{f},g}$, and $\Sigma_{\mathrm{s},l,g'\to g}$ are macroscopic total, fission, and lth order scattering cross sections, respectively; $R_{l,m}(\vec{\Omega})$ is the (l,m)th order spherical harmonic function; NG and NL are the total number of neutron energy groups and the maximum order of Legendre expansion for scattering cross section, respectively; v_g is the neutron velocity of the gth neutron energy group; ω_{p} is the fundamental mode of prompt ω-eigenvalue and corresponds to $\omega_{\mathrm{p}} = -\alpha$; and $\psi_{\mathrm{p},g}(\vec{r},\vec{\Omega})$ is the corresponding eigenfunction of angular neutron flux at the position $\vec{r}$ and direction $\vec{\Omega}$. The calculation of Equation (4) can be carried out by the alpha-search algorithm (or α-k iteration technique) implemented in a deterministic neutron transport code, such as PARTISN [15].

As explained and verified in a previous study [10], the relative sensitivity coefficients of α with respect to perturbations of arbitrary nuclear data σ (hereafter, denoted as $S_{\alpha,\sigma}$) can be estimated based on the first-order perturbation theory.

$$S_{\alpha,\sigma} = \frac{\sigma}{\alpha}\frac{\partial\alpha}{\partial\sigma} = \left(\sigma\,\langle\psi^{\dagger}_{\mathrm{p},g}\left(\frac{\partial\left(\mathbf{A}-\mathbf{F}_{\mathrm{p}}\right)}{\partial\sigma} + \frac{\alpha}{\mathrm{v}_g^2}\frac{\partial \mathrm{v}_g}{\partial\sigma}\right)\psi_{\mathrm{p},g}\rangle\right)\Big/\left(\alpha\,\langle\frac{\psi^{\dagger}_{\mathrm{p},g}\psi_{\mathrm{p},g}}{\mathrm{v}_g}\rangle\right), \tag{7}$$

where the superscript $\dagger$ and bracket $\langle\,\rangle$ indicate adjoint and integral over all phase space, respectively. The adjoint eigenfunction $\psi^{\dagger}_{\mathrm{p},g}$ can be numerically obtained by the adjoint calculation of Equation (4).

The estimated relative sensitivity coefficients are arranged into an $m \times n$ matrix form $\mathbf{S}_{\alpha,\sigma}$, where m and n correspond to the total number of target systems and the total number of perturbed nuclear data, respectively. Using the sandwich formula with the relative covariance matrix of nuclear data $\mathbf{\Sigma}_{\alpha}$ and $\mathbf{S}_{\alpha,\sigma}$, the nuclear-data-induced relative covariance matrix between α values in different target systems is evaluated by

$$\mathbf{\Sigma}_{\alpha} = \mathbf{S}_{\alpha,\sigma}\mathbf{\Sigma}_{\sigma}\mathbf{S}^{T}_{\alpha,\sigma}, \tag{8}$$

where the superscript T represents the transpose of matrix. The square root of the (i,i)th diagonal element in $\mathbf{\Sigma}_\alpha$ indicates the relative uncertainty of α for the ith target system, and the (i,j)th nondiagonal elements are related to the correlations between the ith and jth target systems.

3.2. Calculation conditions

3.2.1. Resonance calculation

In this study, the KUCA ADS benchmark problems were numerically solved by the deterministic method using SCALE6.2.3/CENTRM [13,14] and PARTISN [15]. First, as shown in Figure 2, the fuel and reflector assemblies were simplified into a slablike geometry, where the aluminum (Al) sheath was spatially homogenized to the HEU and Pb plates, and the polyethylene. For the smeared one-dimensional unit cells, the effective microscopic cross sections of HEU, Pb, and polyethylene plates were evaluated by the ultrafine energy group slowing down calculation using SCALE6.2.3/CENTRM with the ENDF/B-VII.1 neutron library [20]. For the reflector assembly and the Al sheath of fully withdrawn control or safety rod cell, the effective microscopic cross sections were evaluated with the infinite homogeneous medium assumption. Consequently, 56 neutron-energy group macroscopic cross sections with P_2 anisotropic scattering matrices were obtained for each material region. The total number of energy groups and the maximum order of anisotropic scattering was determined to carry out the three-dimensional core analysis with practical computational time and memory.

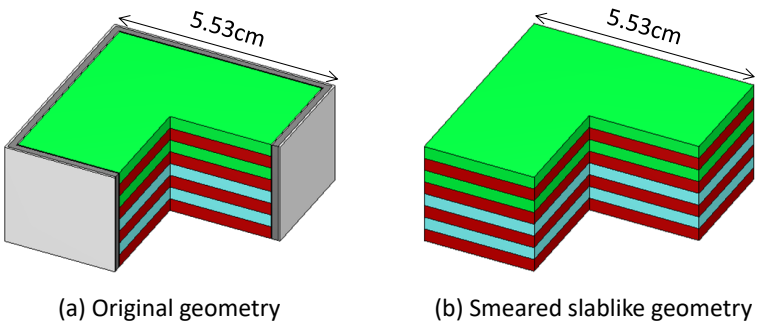

Figure 2. Spatial homogenization for fuel assembly geometry.

3.2.2. Three-dimensional core analysis

The three-dimensional core calculations were performed by the 56 energy-group S_N neutron transport calculation using PARTISN [15], as shown in Figure 3. In the core region, HEU, Pb, and polyethylene plates were treated by a heterogeneous plate-by-plate geometry, and the spatial meshes were axially divided by a 1/16”≈0.16-cm-width unit. Based on the preliminary sensitivity analysis, the thicknesses of axially upper and lower reflectors were approximated by 8”≈20 cm, which were regarded as the sufficient thickness in this study. The spatial meshes in the axial reflectors were divided by a 1-cm-width unit. Four layers of radial reflector assemblies around the core were considered. Each of the fuel and reflector assemblies was radially divided by 4×4 spatial meshes. Air gaps of 0.2-cm width owing to the core support frame were explicitly treated in the core geometry in the PARTISN calculation. To reduce the calculation costs, the 1/2 core symmetry condition for the x-direction was adopted.

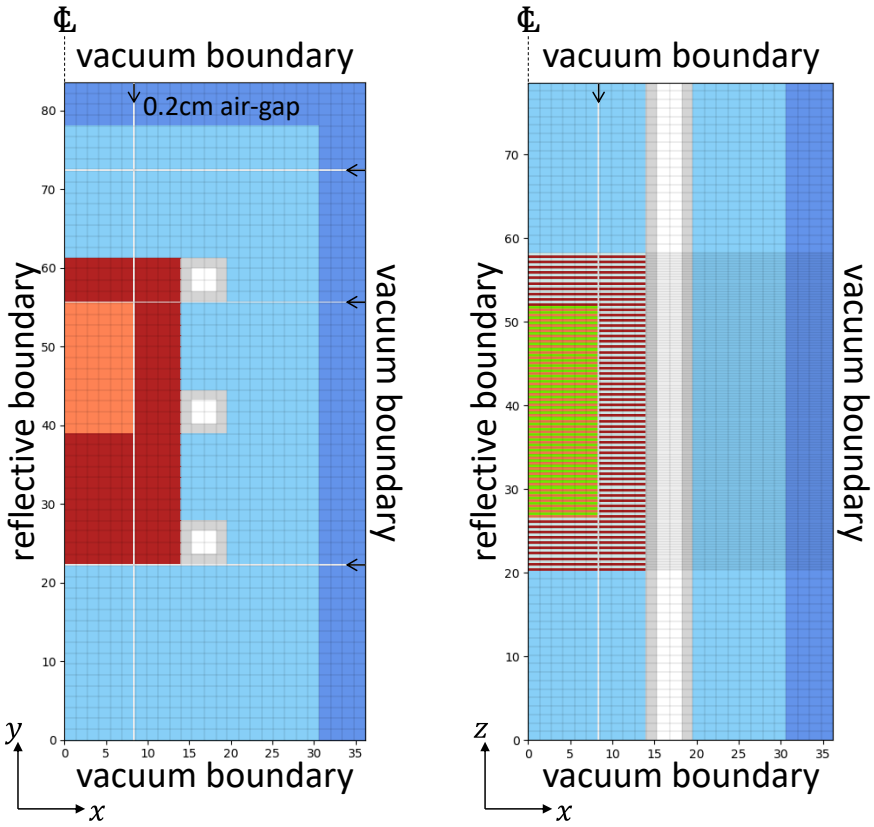

Figure 3. Calculation geometry of PARTISN (4200 HEU plates).

The total number of discretized neutron flight directions $\vec{\Omega}_n = (\Omega_{x,n}, \Omega_{y,n}, \Omega_{z,n})$ was 384 (points/4π) using an improved variant of the EO_N quadrature [21], where the weights and directions are presented in Table S1 and Figure S1 of the supplemental material. The EO_N quadrature is invariant under the octahedral rotation group with inversion. By reconsidering the total number of directions, the combinations of $\vec{\Omega}_n$ and the corresponding weights w_n, the EO_N quadrature was improved. Using the improved EO_N quadrature, numerical integrals of $\int_0^1 d(\cos\theta) \int_0^{\pi/2} d\varphi \left(\Omega_x^i \Omega_y^j \Omega_z^k\right)$ can be accurately calculated by the weighted sum of $\sum_{n=1}^{48} w_n \Omega_{x,n}^i \Omega_{y,n}^j \Omega_{z,n}^k$ for integers i, j, and k within the range of $0 \leq (i+j+k) \leq 10$ (Table S2 of the supplemental material). Thereby, if the angular neutron flux is discontinuous or not smooth at a boundary plane between different material regions, it is expected that the improved EO_N quadrature makes possible the efficient numerical integral of angular flux with respect to $\vec{\Omega}$ (i.e., scalar flux and angular flux moments), in a similar way to the double Gauss-Legendre quadrature for a one-dimensional slab or spherical geometry.

The convergence criteria of the outer and inner iterations are 10^{-7} for k_{eff}-eigenvalue and α-search calculations. The transport sweep was solved by the diamond differencing with a set-to-zero fixup scheme. As described in Reference [9], the PARTISN source code (tnewpa3d.f) was modified to obtain a negative value of ω_{p}. In the case of α-search calculation, prompt components of the production cross section $\nu_{\text{p}}\Sigma_{\text{f}}$ and fission spectrum χ_{p} were used for the prompt ω-calculation. For each of the k_{eff}-eigenvalue and α-search calculations, forward and adjoint calculations were carried out to obtain the forward and adjoint angular flux moment files (rmflux and amflux), where the total number of angular flux moments $\phi_{l,m}$ (namely, expansion coefficients of angular flux by $R_{l,m}(\vec{\Omega})$) was nine: $\phi_{0,0}$, $\phi_{1,0}$, $\phi_{1,1}$, $\phi_{1,-1}$, $\phi_{2,0}$, $\phi_{2,1}$, $\phi_{2,-1}$, $\phi_{2,2}$, and $\phi_{2,-2}$.

3.2.3. SA and UQ

The relative sensitivity coefficients of k_{eff} and α were calculated using an in-house tool based on the first-order perturbation theory. The nine angular flux moments of forward and adjoint fluxes were used for the sensitivity analysis. By comparing the k_{eff}-sensitivity coefficients obtained by MCNP6.2 [22,23] and SCALE6.2.3/TSUNAMI-3D [13,24], the calculation procedure in the in-house tool was preliminarily verified (Figure S2 of the supplemental material). Although the implicit effect in SA by PARTISN was neglected for simplicity, the k_{eff}-sensitivity coefficients by PARTISN agreed well with those by the continuous energy Monte Carlo codes.

To quantify the nuclear data-induced uncertainty of α, the 56 neutron-energy group SCALE covariance library (scale.rev08.56groupcov7.1) was utilized. The covariance data of total fission spectrum χ_g were utilized as alternative covariance data for $\chi_{\text{p},g}$, because $\chi_{\text{p},g}$ is not contained in the SCALE covariance data, and χ_g is roughly equal to $\chi_{\text{p},g}$.

4. Results

4.1. Prompt neutron decay constants

Table 1 summarizes the experimental values of α and numerical results of PARTISN. In addition, Table 1 also presents the forward k_{eff}-eigenvalue, the effective delayed neutron fraction β_{eff} and neutron generation time Λ, where β_{eff} and Λ were calculated based on the conventional definitions using forward and adjoint k_{eff}-eigenfunctions $\psi_{k,g}$ and $\psi_{k,g}^{\dagger}$:

$$\beta_{\text{eff}} = \sum_{i=1}^{6} \frac{\langle \psi_{k,g}^{\dagger} \mathbf{F}_i \psi_{k,g} \rangle}{\langle \psi_{k,g}^{\dagger} \mathbf{F} \psi_{k,g} \rangle}, \tag{9}$$

$$\Lambda = \frac{\langle \psi_{k,g}^{\dagger} \frac{1}{\mathrm{v}_g} \psi_{k,g} \rangle}{\langle \psi_{k,g}^{\dagger} \mathbf{F} \psi_{k,g} \rangle}, \tag{10}$$

where $\mathbf{F}_i$ and $\mathbf{F}$ represent the ith group delayed neutron and the total (prompt and delayed) fission neutron production operators, which are defined in the same manner as Equation (6), respectively.

Table 1. Summary of experimental and numerical results.

HEU plates	experimental results of α (1/s)				numerical results				
	D-T		spallation		α	$\frac{\beta_{\text{eff}}-\rho}{\Lambda}$	k_{eff}	β_{eff}	Λ
	μ_α †	s_α ‡	μ_α	s_α	(1/s)	(1/s)	(-)	(pcm)	(μs)
4440	371.4	4.9	378.3	2.7	464.3	484.8	0.99162	802	33.96
4320	685.3	9.3	697.9	5.4	805.0	864.2	0.97852	805	34.72
4200	1025.2	65.5	1008.6	24.6	1158.5	1285.1	0.96339	808	35.86
4080	1177.9	36.4	1150.9	27.1	1277.7	1426.3	0.95590	807	38.00
3960	N/A	N/A	1233.5	50.9	1329.3	1487.6	0.95220	806	39.17
3840	1690.7	94.4	1643.0	83.6	1803.3	2122.9	0.92623	812	41.34

† weighted arithmetic mean, ‡ square root of weighted sample variance.

As shown in Table 1, the experimental values of α using the D-T and spallation neutron sources were almost the same despite the different energy spectra of PNS. As the subcriticality deepened, the dispersion of measured α tended to increase owing to the spatial dependency of the neutron detectors.

For verification of forward k_{eff} values using the SCALE6.2.3/CENTRM and PARTISN codes, the MCNP6.2 [22] calculation with the ENDF-B/VII.1 library [20] was also carried out (Table S3 of the supplemental material). For example, the MCNP6.2 result of k_{eff} in the 4440 HEU-plates core was 0.99087 ± 0.00004; thus, it was confirmed that the discretization error in the deterministic analysis was relatively small.

The numerical results of α were consistent with the experimental results of μ_α. The biases between the numerical value of α and μ_α were ~120 (1/s). However, the bias between numerical $\frac{\beta_{\text{eff}}-\rho}{\Lambda}$ and experimental μ_α results increased as the subcriticality became deeper. For example, the bias increased to 480 (1/s) in the case of the 3840 HEU-plates core. In other words, if the experimental value of α is simply compared with $\frac{\beta_{\text{eff}}-\rho}{\Lambda}$ converted from the numerical results of k_{eff} and the conventional β_{eff} and Λ, the conversion error results in a larger bias as the subcriticality deepens. This implies that the direct comparison of prompt neutron decay constant α between experimental and numerical results is preferable for the validation in a deeper subcritical system, instead of simple conversion between k_{eff} and α.

4.2. Sensitivity coefficients of α

Figure 4 presents representative relative sensitivity coefficients of α with respect to the nuclear data (microscopic cross sections of elastic scattering cross section reaction σ_{ela}, inelastic scattering reaction $\sigma_{(\text{n,n}')}$, (n,γ) reaction $\sigma_{(\text{n},\gamma)}$, fission reaction σ_{f}, prompt fission spectrum χ_{p}, and number of prompt neutrons per fission ν_{p}) in the case of the 3840 HEU-plates core. In the legends of Figure 4, values between brackets [ ] indicate the energy-integral values of the corresponding sensitivity coefficients. The positive sign of the sensitivity coefficient corresponds to an increase in the magnitude of the prompt neutron decay constant α due to the positive perturbation of nuclear data $+\delta\sigma$, and vice versa.

Figure 4 shows that, in the case of these benchmark problems which are thermal reactor systems despite the presence of the U-Pb zone in the centre of the core, the sensitivity coefficients of α with respect to lead isotopes such as ^{206}Pb were quite small compared with major sensitivity coefficients of the HEU fuel (^{235}U-$\nu_{\text{p}}, \sigma_{\text{f}}, \sigma_{(\text{n},\gamma)}$) and the moderator and reflector of polyethylene (^{1}H-$\sigma_{\text{ela}}, \sigma_{(\text{n},\gamma)}$ and C-σ_{ela}).

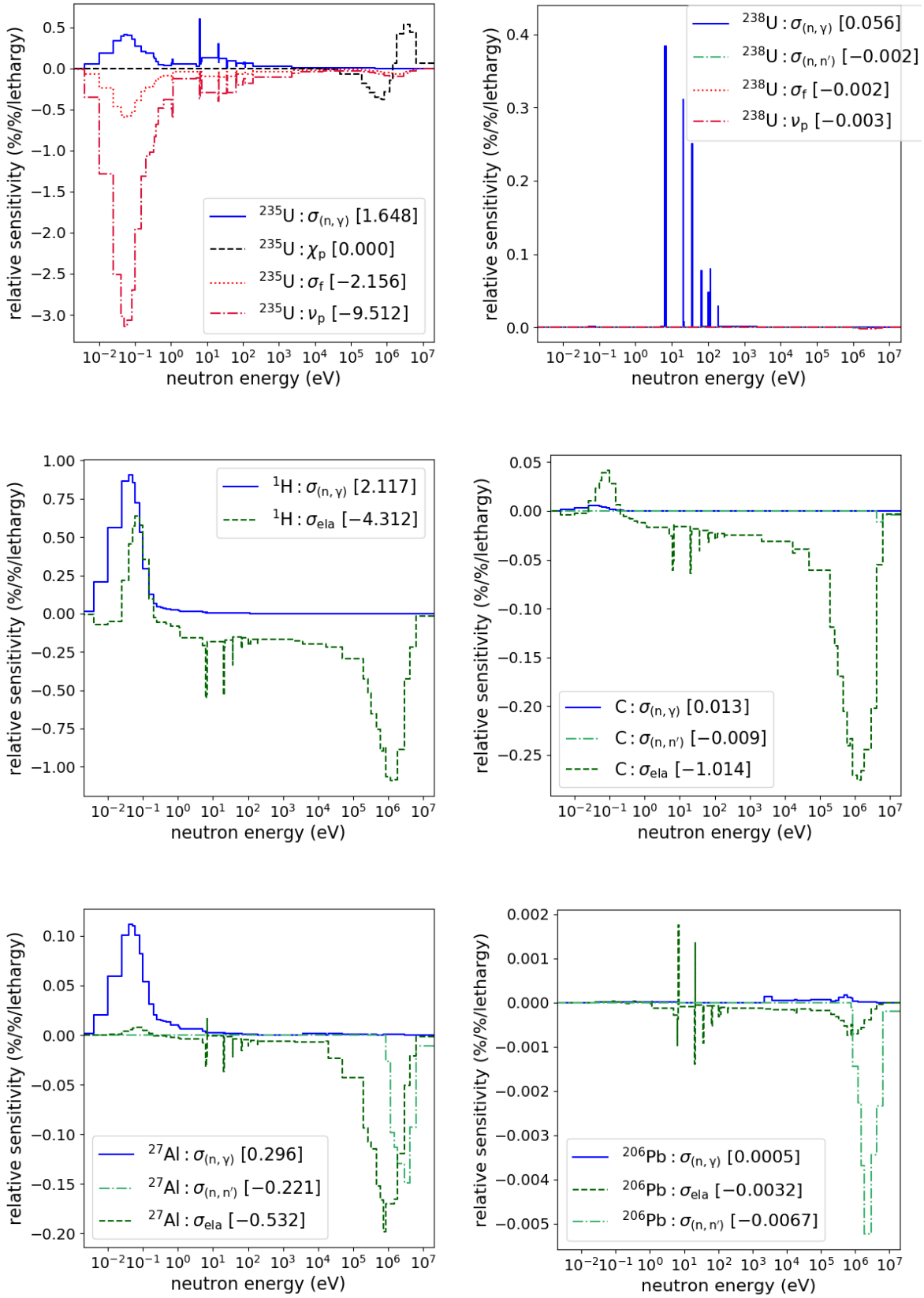

Figure 4. Relative sensitivity coefficients of α (3840 HEU plates).

4.3. Nuclear data-induced uncertainty of α

For each HEU-plates core, Table 2 presents the total nuclear data-induced uncertainty of α and the contributions to the nuclear data-induced α-uncertainty due to each of the covariance data between nuclide-reaction pairs. In Table 2, 'contribution to α-uncertainty' is defined by the square root of the absolute value of the nuclear data-induced covariance of α, and the negative sign of contribution corresponds to the anticorrelation caused by the covariance. For comparison, the contribution to α-uncertainty is presented by the product of the relative uncertainty and the expected value, i.e. absolute uncertainty $\delta\alpha$ (1/s).

Table 2 shows that the total uncertainty of α decreases from 260 to 160 (1/s), as the number of HEU plates decreases, i.e. the subcriticality deepens. Nevertheless, the total nuclear data-induced uncertainties are larger than the dispersions s_α of experimental values. Consequently, the numerical results of α agreed well with the experimental ones within the 1σ ranges of nuclear data-induced uncertainties; namely, the standard differences of $\left|\frac{(\text{numerical result})-(\text{experimental value})}{\text{nuclear data-induced uncertainty}}\right|$ were less than unity. The bias between the numerical $\frac{\beta_{\text{eff}}-\rho}{\Lambda}$ and experimental μ_α results tended to be larger than the nuclear data-induced uncertainty, as the subcriticality deepened. Therefore, this fact strengthened the suggestion that the direct comparison of α between experimental and numerical results is preferable for validation in a deeper subcritical system.

The reason why the total uncertainty decreases is that the substituting reflector assemblies for fuel ones leads to the reduction of major contributions to uncertainty owing to nuclide-reaction pairs of HEU fuel (^{235}U-$\chi_{\text{p}}, \nu_{\text{p}}, \sigma_{(\text{n},\gamma)}$ and ^{27}Al-$\sigma_{\text{ela}}, \sigma_{(\text{n},\text{n}')}$) and polyethylene moderator (^{1}H-σ_{ela}). For the same reason, the contribution of ^{1}H-$\sigma_{(\text{n},\gamma)}$ slightly increases according to the increase of the polyethylene reflector assemblies by the substitution. As with the UQ of k_{eff} for the EE1 core [2], the contributions of ^{27}Al-$\sigma_{\text{ela}}, \sigma_{(\text{n},\text{n}')}$ to the uncertainty of α were comparatively high, because of the high sensitivities of α to the fast energy range shown in Figure 4. Although the contributions of ^{206}Pb, ^{207}Pb, and ^{208}Pb to the uncertainty of

the sample reactivity of the Pb plate was relatively meaningful, as reported in a previous study [25], the contributions of these lead isotopes to the uncertainty of α are negligibly small compared with the major contributions, because the sensitivity coefficients of lead isotopes are very small, as shown in Figure 4.

Table 2. Total nuclear data-induced uncertainty of α and contribution.

Covariance matrix			contribution to α-uncertainty owing to matrix for each HEU-plates core (1/s)					
nuclide-reaction	with	nuclide-reaction	4440	4320	4200	4080	3960	3840
^{235}U-χ_p		^{235}U-χ_p	201.3	186.0	168.2	154.9	148.8	126.0
^{235}U-ν_p		^{235}U-ν_p	97.8	90.0	81.2	75.7	73.2	62.0
^{27}Al-σ_{ela}		^{27}Al-σ_{ela}	63.5	57.7	51.1	45.8	42.8	34.9
^{235}U-$\sigma_{(n,\gamma)}$		^{235}U-$\sigma_{(n,\gamma)}$	60.3	55.9	50.8	46.9	45.0	38.5
^{27}Al-$\sigma_{(n,n')}$		^{27}Al-$\sigma_{(n,n')}$	52.1	48.2	43.5	39.2	37.1	31.4
^{1}H-σ_{ela}		^{1}H-σ_{ela}	49.3	45.6	41.2	37.8	36.4	30.7
^{1}H-$\sigma_{(n,\gamma)}$		^{1}H-$\sigma_{(n,\gamma)}$	38.8	39.1	39.3	39.9	40.2	40.7
^{235}U-σ_f		^{235}U-$\sigma_{(n,\gamma)}$	27.8	25.5	22.8	21.3	20.6	17.3
^{27}Al-$\sigma_{(n,\gamma)}$		^{27}Al-$\sigma_{(n,\gamma)}$	19.5	18.5	17.2	16.2	15.7	14.2
^{235}U-σ_f		^{235}U-σ_f	18.7	16.9	14.9	14.0	13.5	11.1
C-σ_{ela}		C-σ_{ela}	16.6	15.4	14.0	12.9	12.5	10.7
C-$\sigma_{(n,n')}$		C-$\sigma_{(n,n')}$	6.5	6.0	5.4	5.1	4.9	4.2
C-σ_{ela}		C-$\sigma_{(n,n')}$	-6.5	-6.0	-5.4	-5.0	-4.9	-4.2
^{235}U-σ_{ela}		^{235}U-$\sigma_{(n,\gamma)}$	5.8	5.3	4.6	4.0	3.7	2.9
^{235}U-$\sigma_{(n,n')}$		^{235}U-$\sigma_{(n,n')}$	5.0	4.6	4.2	3.7	3.5	2.9
^{234}U-$\sigma_{(n,\gamma)}$		^{234}U-$\sigma_{(n,\gamma)}$	2.6	2.4	2.2	1.9	1.8	1.5
^{235}U-$\sigma_{(n,n')}$		^{235}U-σ_{ela}	-2.3	-2.0	-1.8	-1.6	-1.5	-1.2
^{238}U-$\sigma_{(n,\gamma)}$		^{238}U-$\sigma_{(n,\gamma)}$	1.7	1.6	1.4	1.3	1.2	1.0
^{238}U-$\sigma_{(n,n')}$		^{238}U-$\sigma_{(n,n')}$	1.1	1.0	0.9	0.8	0.8	0.7
^{206}Pb-$\sigma_{(n,n')}$		^{206}Pb-$\sigma_{(n,n')}$	1.1	1.1	1.1	1.0	1.0	0.9
^{235}U-σ_{ela}		^{235}U-σ_f	1.0	1.1	1.1	1.1	1.1	1.0
^{235}U-σ_{ela}		^{235}U-σ_{ela}	1.0	0.9	0.8	0.7	0.6	0.5
^{208}Pb-$\sigma_{(n,n')}$		^{208}Pb-$\sigma_{(n,n')}$	0.9	0.9	0.9	0.8	0.8	0.7
^{207}Pb-$\sigma_{(n,n')}$		^{207}Pb-$\sigma_{(n,n')}$	0.8	0.8	0.8	0.8	0.7	0.7
^{208}Pb-σ_{ela}		^{208}Pb-σ_{ela}	0.7	0.6	0.5	0.5	0.4	0.3
Total			**257.4**	**238.0**	**215.7**	**199.2**	**191.6**	**163.6**

5. Conclusion

In this study, a numerical analysis of the prompt neutron decay constant α using the deterministic calculation codes SCALE6.2.3/CENTRM and PARTISN was carried out for the U-Pb zoned cores in the KUCA ADS benchmark problems. In addition, the nuclear data-induced uncertainty of α was quantified by an efficient numerical method based on the first-order perturbation theory. Consequently, the numerical results of α agreed well with the experimental results obtained by the PNS method within the 1σ ranges of nuclear data-induced uncertainties. Thus, it was reconfirmed that the measurement results of α reported in the KUCA ADS benchmark problems are useful to validate the prompt ω-eigenvalue calculation. Furthermore, it was clarified that the major contributions to the uncertainty of α were the nuclide-reaction pairs of HEU fuel (^{235}U-$\chi_{\mathrm{p}}, \nu_{\mathrm{p}}, \sigma_{(\mathrm{n},\gamma)}$ and ^{27}Al-$\sigma_{\mathrm{ela}}, \sigma_{(\mathrm{n},\mathrm{n}')}$) and polyethylene (^{1}H-$\sigma_{\mathrm{ela}}, \sigma_{(\mathrm{n},\gamma)}$). However, in these KUCA benchmark problems, the contributions of the lead isotopes to the uncertainty of α are negligibly small compared with the major contributions.

In this study, the implicit effect in SA by PARTISN was neglected for simplicity, because the impact of the implicit effect on UQ seemed to be relatively small in the case of HEU fuel loaded in KUCA cores, compared with a typical low enriched uranium fuel in a thermal reactor system. For more-rigorous UQ of α, the treatment of the implicit effect in SA of α is a subject for future investigation. Furthermore, in the case of the deterministic code, it is also an important issue to quantify appropriately or to reduce reasonably the discretization error of α for the thorough UQ. To address these problems, further research and development for SA of α using a continuous energy Monte Carlo code are needed. Recently, the numerical methodologies for SA of α using the Monte Carlo method have been investigated [26,27]; thus, these sophisticated methodologies are helpful for future investigations.

References

1. Pyeon CH, Yamanaka M, Kim SH. Benchmarks of subcriticality in accelerator-driven system at Kyoto University Critical Assembly. Nucl Eng Technol. 2017;49(6):1234–1239.
2. Yamanaka M, Pyeon CH. Benchmarks of criticality in solid-moderated and solid-reflected cores at Kyoto University Critical Assembly. Nucl Sci Eng. 2019;193(4):404–416.
3. Pyeon CH, editor. Experimental benchmarks for Accelerator-Driven System (ADS) at Kyoto University Critical Assembly. Kyoto: Kyoto University Institute for Integrated Radiation and Nuclear Science; 2012. KURRI-TR-444. Available from: https://www.rri.kyoto-u.ac.jp/PUB/report/03_tr_backnumber/img/KURRI-TR-444.pdf
4. Pyeon CH, editor. Experimental benchmarks on thorium-loaded accelerator-driven system at Kyoto University Critical Assembly. Kyoto: Kyoto University Institute for Integrated Radiation and Nuclear Science; 2015. KURRI-TR(CD)-48. Available from: https://www.rri.kyoto-u.ac.jp/PUB/report/04_cd/img/KURRI-TR-48.pdf
5. Pyeon CH, editor. Experimental benchmarks of neutronics on solid Pb-Bi in accelerator-driven system with 100 MeV protons at Kyoto University Critical Assembly. Kyoto: Kyoto University Institute for Integrated Radiation and Nuclear Science; 2017. KURRI-TR-447. Available from: https://www.rri.kyoto-u.ac.jp/PUB/report/03_tr/img/KUCA_ADS-CRP2016.pdf
6. Pyeon CH, Yamanaka M, editors, Experimental benchmarks of neutron characteritics on uranium-lead zoned core in accelerator-driven system at Kyoto University Critical Assembly. Kyoto: Kyoto University Institute for Integrated Radiation and Nuclear Science; 2018. KURNS-EKR-001. Available from: https://www.rri.kyoto-u.ac.jp/PUB/report/09_kurns/temp/kurns-ekr-001.pdf
7. Lagrange JB, Planche T, Yamakawa E, et al. Straight scaling FFAG beam line. Nucl Instrum Methods Phys Res A. 2012;691:55–63.
8. Yamakawa E, Uesugi T, Lagrange JB, et al. Serpentine acceleration in zero-chromatic

FFAG accelerators. Nucl Instrum Methods Phys Res A. 2013;716:46–53.

9. Endo T, Chiba G, van Rooijen W.F.G, et al. Experimental analysis and uncertainty quantification using random sampling technique for ADS experiments at KUCA. J Nucl Sci Technol. 2018;55(4):450–459.
10. Endo T, Yamamoto A. Sensitivity analysis of prompt neutron decay constant using perturbation theory. J Nucl Sci Technol. 2018;55(11):1245–1254.
11. Pitts M, Rahnema F, Williamson TG, et al. Water-reflected 91-liter sphere of enriched uranium oxyfluoride solution. Paris: OECD Nuclear Energy Agency; 2004. NEA/NSC/DOC/(95)03/II, Volume II, HEU-SOL-THERM-012, revision 3.
12. Pyeon CH, Yamanaka M, Ito Makoto, et al. Uncertainty quantification of criticality in solid-moderated and -reflected cores at Kyoto University Critical Assembly. J Nucl Sci Technol. 2018;55(7):812–821.
13. Rearden BT, Jessee MA, editors. SCALE code system. Oak Ridge (TN): Oak Ridge National Laboratory; 2018. ORNL/TM-2005/39 Version 6.2.3.
14. Williams ML. Resonance self-shielding methodologies in SCALE 6. Nucl Technol. 2011;174(2):149–168.
15. Alcouffe RE, Baker RS, Dahl JA, et al. PARTISN: a time-dependent, parallel neutral particle transport code system. Los Alamos (NM): Los Alamos National Laboratory; 2008. LA-UR-08-07258.
16. Simmons BE, King JS. A pulsed neutron technique for reactivity determination. Nucl Sci Eng. 1958;3(5):595–608.
17. Kitamura Y, Pázsit, I, Wright J, et al. Calculation of the pulsed Feynman- and Rossi-alpha formulae with delayed neutrons. Ann Nucl Energy. 2005;32(3):671–692.
18. Yagi T, Pyeon CH, Misawa T. Application of wavelength shifting fiber to subcriticality measurements. Appl Radiat Isot. 2013;72:11–15.
19. Watanabe K, Kawabata Y, Yamazaki A, et al. Development of an optical fiber type detector

using a Eu:LiCaAlF6 scintillator for neutron monitoring in boron neutron capture therapy. Nucl Instrum Methods Phys Res A. 2015;802:1–4.

20. Chadwick MB, Herman M, Obložinský P, et al. ENDF/B-VII.1 nuclear data for science and technology: cross sections, covariances, fission product yields and decay data. Nucl Data Sheets. 2011;112(12):2887–2996.
21. Endo T, Yamamoto A. Development of new solid angle quadrature sets to satisfy even- and odd-moment conditions. J Nucl Sci Technol. 2007;44(10):1249–1258.
22. Werner CJ, editor. MCNP User's manual code version 6.2. Los Alamos (NM): Los Alamos National Laboratory; 2017. LA-UR-17-29981.
23. Kiedrowski BC, Brown FB, Wilson PPH. Adjoint-weighted tallies for *k*-eigenvalue calculations with continuous-energy Monte Carlo. Nucl Sci Eng. 2011;168(3):226–241.
24. Perfetti CM, Rearden BT, Martin WR. SCALE continuous-energy eigenvalue sensitivity coefficient calculations. Nucl Sci Eng. 2016;182(3):332–353.
25. Pyeon CH, Fujimoto A, Sugawara T, et al. Sensitivity and uncertainty analyses of lead sample reactivity experiments at Kyoto University Critical Assembly. Nucl Sci Eng. 2017;185(3):460–472.
26. Terranova N, Zoia A. Generalized iterated fission probability for Monte Carlo eigenvalue calculations. Ann Nucl Energy. 2017;108:57–66.
27. Yamamoto T, Sakamoto H. A Monte Carlo technique for sensitivity analysis of alpha-eigenvalue with the differential operator sampling method. Ann Nucl Energy. 2019;127:178–187.

Supplemental Online Material

Table S1. Improved EO_N quadrature of 384 (points/4π). The 48 discretized directions over an octant of the sphere are presented in the following table.

n	weight w_n[†]	$\Omega_{x,n}$	$\Omega_{y,n}$	$\Omega_{z,n}$
1	2.7133901557034558e-4	2.2250255888577393e-2	2.2250255888577393e-2	9.9950480350310756e-1
2	2.7133901557034558e-4	2.2250255888577393e-2	9.9950480350310756e-1	2.2250255888577393e-2
3	2.7133901557034558e-4	9.9950480350310756e-1	2.2250255888577393e-2	2.2250255888577393e-2
4	2.4747658377021711e-3	1.5063842157143472e-1	1.5063842157143472e-1	9.7704459053460473e-1
5	2.4747658377021711e-3	1.5063842157143472e-1	9.7704459053460473e-1	1.5063842157143472e-1
6	2.4747658377021711e-3	9.7704459053460473e-1	1.5063842157143472e-1	1.5063842157143472e-1
7	3.1302276351586317e-3	5.2345326834952976e-1	5.2345326834952976e-1	6.7230450817199669e-1
8	3.1302276351586317e-3	5.2345326834952976e-1	6.7230450817199669e-1	5.2345326834952976e-1
9	3.1302276351586317e-3	6.7230450817199669e-1	5.2345326834952976e-1	5.2345326834952976e-1
10	4.3735792205142644e-3	3.6464927043714109e-1	3.6464927043714109e-1	8.5677407707009990e-1
11	4.3735792205142644e-3	3.6464927043714109e-1	8.5677407707009990e-1	3.6464927043714109e-1
12	4.3735792205142644e-3	8.5677407707009990e-1	3.6464927043714109e-1	3.6464927043714109e-1
13	8.6581574778795299e-4	9.9164907955830643e-1	1.2591820170388069e-1	2.7869508263054451e-2
14	8.6581574778795299e-4	9.9164907955830643e-1	2.7869508263054451e-2	1.2591820170388069e-1
15	8.6581574778795299e-4	1.2591820170388069e-1	2.7869508263054451e-2	9.9164907955830643e-1
16	8.6581574778795299e-4	1.2591820170388069e-1	9.9164907955830643e-1	2.7869508263054451e-2
17	8.6581574778795299e-4	2.7869508263054451e-2	9.9164907955830643e-1	1.2591820170388069e-1
18	8.6581574778795299e-4	2.7869508263054451e-2	1.2591820170388069e-1	9.9164907955830643e-1
19	1.5472421060451036e-3	2.7641148244519852e-2	3.2807233804759719e-1	9.4424811778033616e-1
20	1.5472421060451036e-3	2.7641148244519852e-2	9.4424811778033616e-1	3.2807233804759719e-1
21	1.5472421060451036e-3	3.2807233804759719e-1	9.4424811778033616e-1	2.7641148244519852e-2
22	1.5472421060451036e-3	3.2807233804759719e-1	2.7641148244519852e-2	9.4424811778033616e-1
23	1.5472421060451036e-3	9.4424811778033616e-1	2.7641148244519852e-2	3.2807233804759719e-1
24	1.5472421060451036e-3	9.4424811778033616e-1	3.2807233804759719e-1	2.7641148244519852e-2
25	2.3832288775456662e-3	8.0884418745966909e-1	3.8677548893897996e-2	5.8674962941979590e-1
26	2.3832288775456662e-3	8.0884418745966909e-1	5.8674962941979590e-1	3.8677548893897996e-2
27	2.3832288775456662e-3	3.8677548893897996e-2	5.8674962941979590e-1	8.0884418745966909e-1
28	2.3832288775456662e-3	3.8677548893897996e-2	8.0884418745966909e-1	5.8674962941979590e-1
29	2.3832288775456662e-3	5.8674962941979590e-1	8.0884418745966909e-1	3.8677548893897996e-2
30	2.3832288775456662e-3	5.8674962941979590e-1	3.8677548893897996e-2	8.0884418745966909e-1
31	3.5205752634728772e-3	7.3867548144924025e-1	3.5409633503112433e-1	5.7356282883678827e-1
32	3.5205752634728772e-3	7.3867548144924025e-1	5.7356282883678827e-1	3.5409633503112433e-1
33	3.5205752634728772e-3	3.5409633503112433e-1	5.7356282883678827e-1	7.3867548144924025e-1
34	3.5205752634728772e-3	3.5409633503112433e-1	7.3867548144924025e-1	5.7356282883678827e-1
35	3.5205752634728772e-3	5.7356282883678827e-1	7.3867548144924025e-1	3.5409633503112433e-1
36	3.5205752634728772e-3	5.7356282883678827e-1	3.5409633503112433e-1	7.3867548144924025e-1
37	3.6575247841537903e-3	1.5970861147690090e-1	3.6166764655266084e-1	9.1852581501946907e-1
38	3.6575247841537903e-3	1.5970861147690090e-1	9.1852581501946907e-1	3.6166764655266084e-1
39	3.6575247841537903e-3	3.6166764655266084e-1	9.1852581501946907e-1	1.5970861147690090e-1
40	3.6575247841537903e-3	3.6166764655266084e-1	1.5970861147690090e-1	9.1852581501946907e-1
41	3.6575247841537903e-3	9.1852581501946907e-1	1.5970861147690090e-1	3.6166764655266084e-1
42	3.6575247841537903e-3	9.1852581501946907e-1	3.6166764655266084e-1	1.5970861147690090e-1
43	3.7339906998552367e-3	5.9296347373652011e-1	7.8514467677154377e-1	1.7872368436115927e-1
44	3.7339906998552367e-3	5.9296347373652011e-1	1.7872368436115927e-1	7.8514467677154377e-1
45	3.7339906998552367e-3	7.8514467677154377e-1	1.7872368436115927e-1	5.9296347373652011e-1
46	3.7339906998552367e-3	7.8514467677154377e-1	5.9296347373652011e-1	1.7872368436115927e-1
47	3.7339906998552367e-3	1.7872368436115927e-1	5.9296347373652011e-1	7.8514467677154377e-1
48	3.7339906998552367e-3	1.7872368436115927e-1	7.8514467677154377e-1	5.9296347373652011e-1

[†] Total sum of weights is normalized as $\sum_{n=1}^{48} w_n = \frac{1}{8}$.

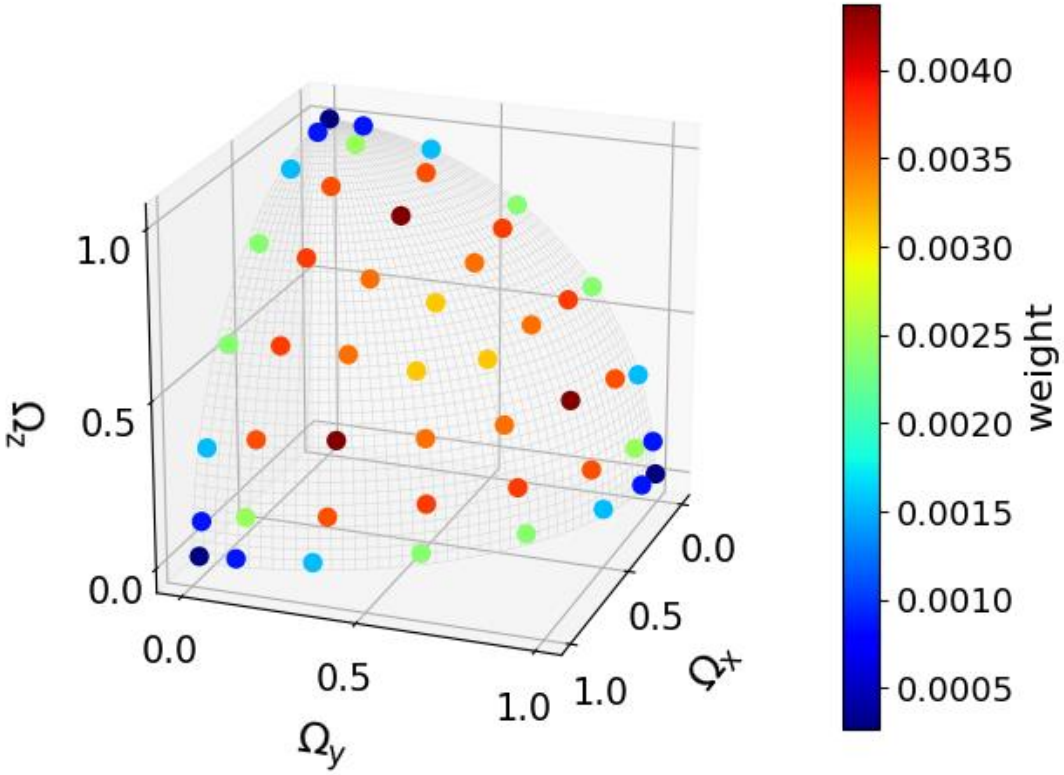

Figure S1. Improved EO_N quadrature of 384 (points/4π).

Table S2. Analytical values of $I_{ijk} = \int_0^1 d(\cos\theta) \int_0^{\pi/2} d\varphi \left(\Omega_x^i \Omega_y^j \Omega_z^k\right)$.

(i,j,k)	I_{ijk}
0 0 0	π/2
1 0 0	π/4
2 0 0	π/6
1 1 0	1/3
3 0 0	π/8
2 1 0	π/16
1 1 1	1/8
4 0 0	π/10
3 1 0	2/15
2 2 0	π/30
2 1 1	1/15
5 0 0	π/12
4 1 0	π/32
3 2 0	π/48
3 1 1	1/24
2 2 1	π/96

(i,j,k)	I_{ijk}
6 0 0	π/14
5 1 0	8/105
4 2 0	π/70
3 3 0	4/105
4 1 1	1/35
3 2 1	2/105
2 2 2	π/210
7 0 0	π/16
6 1 0	5π/256
5 2 0	π/96
4 3 0	π/128
5 1 1	1/48
4 2 1	π/256
3 3 1	1/96
3 2 2	π/384

(i,j,k)	I_{ijk}
8 0 0	π/18
7 1 0	16/315
6 2 0	π/126
5 3 0	16/945
6 1 1	1/63
4 4 0	π/210
5 2 1	8/945
4 3 1	2/315
4 2 2	π/630
3 3 2	4/945
9 0 0	π/20
8 1 0	7π/512
7 2 0	π/160
7 1 1	1/80
6 3 0	π/256
5 4 0	π/320
6 2 1	π/512
5 3 1	1/240
4 4 1	3π/2560
5 2 2	π/960
4 3 2	π/1280
3 3 3	1/480

(i,j,k)	I_{ijk}
10 0 0	π/22
9 1 0	128/3465
8 2 0	π/198
8 1 1	1/99
7 3 0	32/3465
6 4 0	π/462
5 5 0	64/10395
7 2 1	16/3465
6 3 1	2/693
5 4 1	8/3465
6 2 2	π/1386
5 3 2	16/10395
4 4 2	π/2310
4 3 3	4/3465

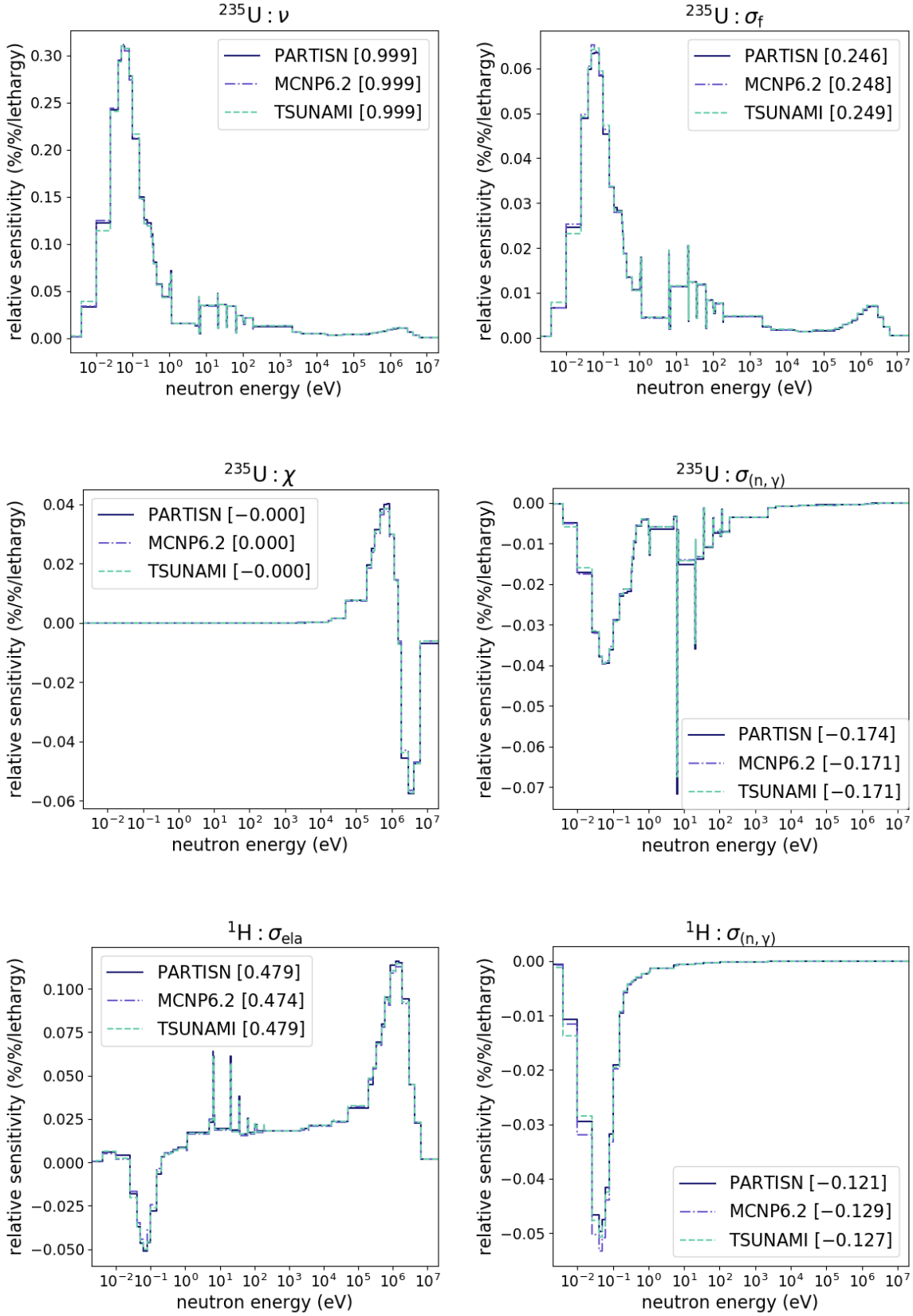

Figure S2. Comparison of relative sensitivity coefficients of k_{eff} among PARTISN, MCNP6.2, and TSUNAMI-3D (4440 HEU plates).

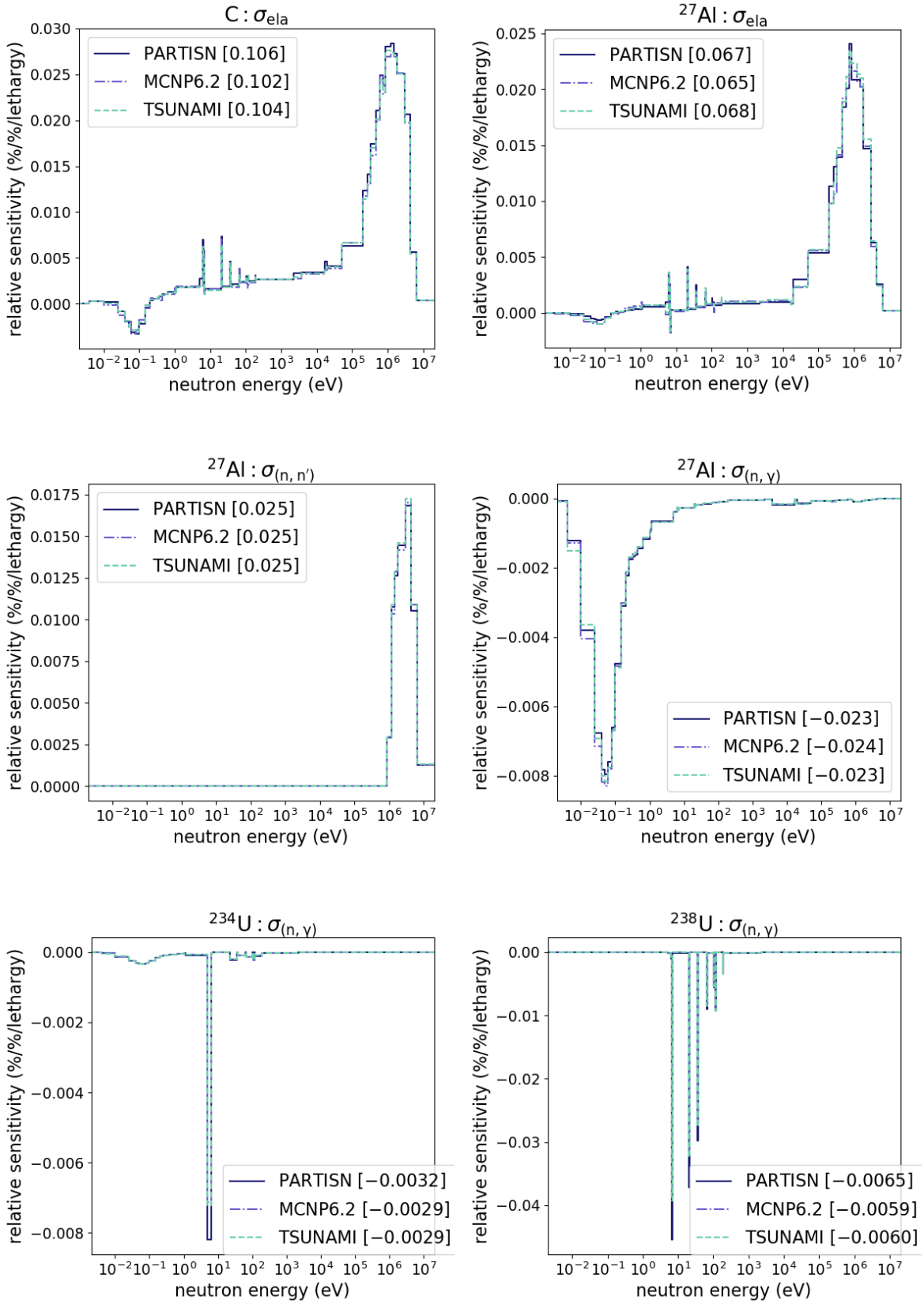

Figure S2. Comparison of relative sensitivity coefficients of k_{eff} among PARTISN, MCNP6.2, and TSUNAMI-3D (4440 HEU plates) (continued).

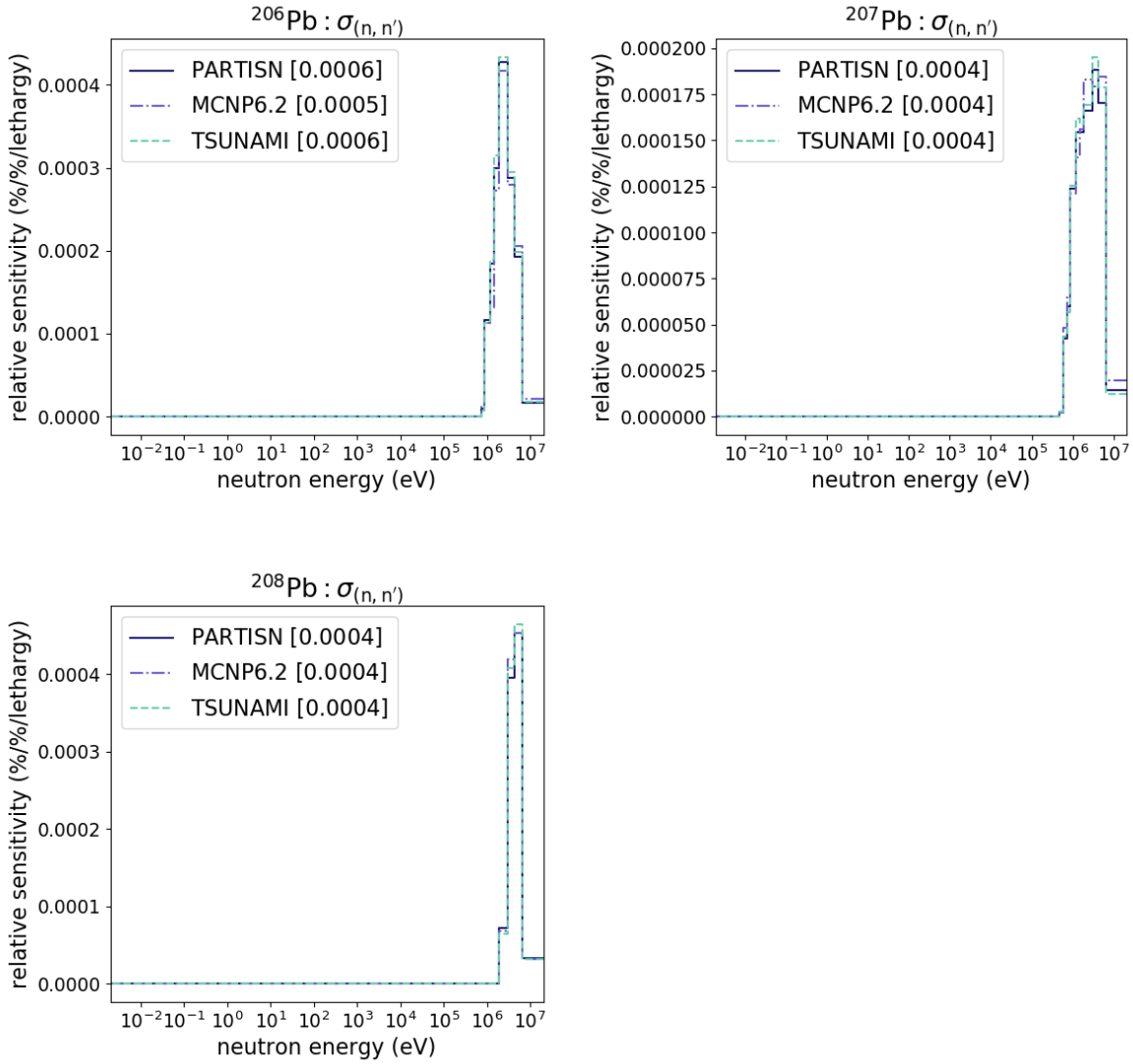

Figure S2. Comparison of relative sensitivity coefficients of k_{eff} among PARTISN, MCNP6.2, and TSUNAMI-3D (4440 HEU plates) (continued).

Calculation conditions:

MCNP6.2: as-built geometry, ENDF-B/VII.1, IFP method, nsrck=50000, ikz=400, kct=10400, blocksize=5;

TSUNAMI-3D: as-built geometry, ENDF-B/VII.1, CE CLUTH method, npg=50000, gen=10400, nsk=400, cfp=5.

Table S3. Numerical results of MCNP6.2.

EU plates	k_{eff} (-)	β_{eff} (pcm)	Λ (μs)
4440	0.99087 ± 0.00004[†]	795 ± 3	35.310 ± 0.020
4320	0.97861 ± 0.00004	802 ± 3	36.097 ± 0.021
4200	0.96438 ± 0.00004	803 ± 3	37.149 ± 0.021
4080	0.95624 ± 0.00004	802 ± 3	39.253 ± 0.022
3960	0.95182 ± 0.00004	807 ± 3	40.388 ± 0.022
3840	0.92801 ± 0.00004	806 ± 3	42.486 ± 0.024

[†]1σ statistical error.

Calculation conditions:

MCNP6.2: as-built geometry, ENDF-B/VII.1, IFP method, nsrck=50000, ikz=400, kct=10400, blocksize=5.